




RESEARCH ARTICLE

The role of Meteorin-like in skeletal development and bone fracture healing

Rong Huang^{1,2}  | Abhinav R. Balu^{1,2} | Kristin H. Molitoris^{1,2} | James P. White¹ | Alexander G. Robling³ | Ugur M. Ayturk^{4,5}  | Gurpreet S. Baht^{1,2,6} 

¹Department of Medicine, Duke Molecular Physiology Institute, Durham, North Carolina, USA

²Department of Orthopaedic Surgery, Duke University, Durham, North Carolina, USA

³Department of Anatomy and Cell Biology, Indiana University School of Medicine, Indianapolis, Indiana, USA

⁴Department of Research, Hospital for Special Surgery, New York City, New York, USA

⁵Department of Orthopaedic Surgery, Weill Cornell Medicine, New York City, New York, USA

⁶Department of Pathology, Duke University, Durham, North Carolina, USA

Correspondence

Gurpreet S. Baht, Department of Medicine, Duke Molecular Physiology Institute, 300 North Duke Street, Durham, NC 27701, USA. Email: gurpreet.baht@duke.edu

Ugur M. Ayturk, Hospital for Special Surgery (HSS), 535 East 70th St. New York City, NY 10021, USA. Email: ayturku@hss.edu

Abstract

Meteorin-like protein (*Metrl*), homologous to the initially identified neurotrophic factor Meteorin, is a secreted, multifunctional protein. Here we used mouse models to investigate *Metrl*'s role in skeletal development and bone fracture healing. During development *Metrl* was expressed in the perichondrium and primary ossification center. In neonates, single cell RNA-seq of diaphyseal bone demonstrated strongest expression of *Metrl* transcript by osteoblasts. In vitro, *Metrl* was osteoinductive, increasing osteoblast differentiation and mineralization in tissue culture models. In vivo, loss of *Metrl* expression resulted in no change in skeletal metrics in utero, at birth, or during postnatal growth. Six-week-old *Metrl*-null mice displayed similar body length, body weight, tibial length, femoral length, BV/TV, trabecular number, trabecular thickness, and cortical thickness as littermate controls. In 4-month-old mice, lack of *Metrl* expression did not change structural stiffness, ultimate force, or energy to fracture of femora under 3-point-bending. Last, we investigated the role of *Metrl* in bone fracture healing. *Metrl* expression increased in response to tibial injury, however, loss of *Metrl* expression did not affect the amount of bone deposited within the healing tissue nor did it change the structural parameters of healing tissue. This work identifies *Metrl* as a dispensable molecule for skeletal development. However, the osteoinductive capabilities of *Metrl* may be utilized to modulate osteoblast differentiation in cell-based orthopedic therapies.

KEYWORDS

bone, fracture healing, Meteorin-like, osteoblast, skeletal development

Abbreviations: Alp, alkaline phosphatase; BMSC, bone marrow stromal cell; BSP, bone sialoprotein; BV, bone volume; Col1, type I collagen; Ct. Th, cortical thickness; E15.5, embryos on day 15.5 of gestation; E18.5, embryos on day 18.5 of gestation; HET, heterozygote; KO, knockout; *Metrl*, Meteorin-like protein; Ocn, osteocalcin; Opn, osteopontin; r*Metrl*, recombinant Meteorin-like protein; SIBLING, small, integrin-binding ligand N-linked glycoprotein; Tb. N, trabecular number; Tb. Th, trabecular thickness; TMD, bone mineral density; TV, total volume; VK, Von Kossa; WT, wildtype.

This is an open access article under the terms of the Creative Commons Attribution-NoDerivs License, which permits use and distribution in any medium, provided the original work is properly cited and no modifications or adaptations are made.

© 2022 The Authors. *Journal of Orthopaedic Research*® published by Wiley Periodicals LLC on behalf of Orthopaedic Research Society.

1 | INTRODUCTION

Bone development, growth, and regeneration involve an intricate network of cells and secreted factors. A large body of work has been performed to identify signaling proteins that alter bone biology in an effort to harness their function for therapeutic advancement. Over the last decade, significant advances in protein identification technology have led to better identification of previously undetected signaling molecules, such as Meteorin-like protein (*Metrnl*). Using parabiosis and conditioned-media models, we recently identified *Metrnl* to be among a group of proteins that could potentially affect osteoblast activity and thereby, bone biology.¹ Indeed, recent findings have indicated that viral induction of *Metrnl* expression alters in vitro osteoblast differentiation and activity.²

Metrnl was first identified as a secreted adipokine with homology to the neurotrophic factor Meteorin protein.³ The functions of *Metrnl* are still being delineated. Early studies have identified *Metrnl* to have a role in white adipose browning, insulin sensitization, and recently we identified *Metrnl* to be critical in resolution of inflammation following muscle injury.⁴⁻⁸ Loss of *Metrnl* expression led to prolonged inflammation at the site of injury and impaired muscle healing. *Metrnl* is expressed in abundance by muscle tissue; however, despite the close anatomical proximity to bone and the established cross-talk between muscle and bone, the role of *Metrnl* in bone biology is not known.⁹⁻¹¹

Here we describe the skeletal expression pattern of *Metrnl* during pre and postnatal development and bone fracture healing. Furthermore, by utilizing two independently generated knockout mouse models, we interrogate the role of *Metrnl* in these biological processes. Our results indicate that, despite its relatively high expression in osteoblasts, *Metrnl* is dispensable for normal bone mass accumulation, biomechanical strength and healing in mice.

2 | MATERIALS AND METHODS

2.1 | Mouse models

All methods performed within this study were approved by the Institutional and Animal Care and Use Committees of Duke University and Boston Children's Hospital. We used two *Metrnl*^{-/-} mouse models in our experiments. Both models were mated with C57BL/6J (Stock No. 000664) mice purchased from Jackson Labs. *Metrnl*^{+/-} progeny were used as breeders to generate *Metrnl*^{-/-} (knockout, KO), *Metrnl*^{+/-} (heterozygous, Het), and *Metrnl*^{+/+} (wildtype, WT) littermates for subsequent analysis.

The first model was originally generated by Lexicon Pharmaceuticals¹² and generously provided to us by Dr. Bruce Spiegelman. Genotype was verified using DNA PCR of tail fragments using a combination of common primer (5'-GCCTAGCCGAGGGAGAGCCG-3'), wildtype primer (5'-TGTGACTTGGGAGCTCTGCAGC-3'), and/or mutant primer (5'-GCCGCCCGACTGCATCT-3'). These transgenic mice were used for skeletal development studies, micro-computed

tomography (μ CT) analysis of adult bones, fracture analysis, and BMSC differentiation studies.

The second model was generated by injection of genetically modified embryonic stem cells purchased from the Knockout Mouse Project at University of California Davis into female mouse blastocysts. The chimeric progeny were screened for the correct genotype, (wherein the 2nd exon of *Metrnl* was deleted, leading to a frameshift and nonsense-mediated messenger RNA decay) and further bred on a C57BL/6J background to generate F1 mutant mice. This mouse strain was used for μ CT analysis of adult bones, biomechanical testing of intact bones, and RNA-seq experiments.

2.2 | BMSC culture and differentiation

Metrnl^{+/+} and *Metrnl*^{-/-} mice were euthanized at 4 months of age and the femurs and tibiae were dissected and cleaned of soft tissues. Bone marrow was flushed from the long bone cavities and cells were plated at a density of $500 \times 10^3/\text{cm}^2$ in plating medium (AMEM, 10% fetal bovine serum [FBS], 100 U/ml Penn/Strep) for 10 days. Cells were then differentiated to osteoblasts in osteogenic medium (AMEM, 10% FBS, 100 U/ml Penn/Strep, 30 μ M ascorbic acid, 10^{-8} M dexamethasone, 8 mM sodium phosphate) either with or without 100 ng/ml of r*Metrnl* (R&D Inc.). After 10 days in osteogenic media, wells were washed with PBS, fixed using 10% formalin, and stained for alkaline phosphatase (ALP) using FastRed (Sigma Inc.) or for mineral using Von Kossa.¹³ Relative ALP activity was determined using a p-nitrophenylphosphate based substrate system (Sigma) followed by quenching of the reaction with 3N NaOH and optical density measurement at 405 nm. Relative Von Kossa staining was determined using a surface area measurement, similar to previously published data.¹³ Replicate wells were washed with PBS and RNA was extracted using TRIzol Reagent (Invitrogen Inc.) as per manufacturer's protocol.

2.3 | Real-time PCR

After RNA extraction, purity and quantity of RNA were determined using spectrometric methods. Complementary DNA template was generated using random hexamers. RT-PCR was performed using PowerUp SYBr Green Master Mix (Applied Biosystem) and primers were purchased from Applied Biosystems—Alkaline phosphatase (*Alp*) (forward: 5'-GGACAGGACACACACACA-3', reverse: 5'-CA AACAGGAGAGCCACTTCA-3'), type I collagen (*Col1*) (forward: 5'-CACCCCAATCTGGTCCCTC-3', reverse: 5'-CATAAGCCAAGTG GGCAGGA-3'), and osteocalcin (*Ocn*) (forward: 5'-GAACAGACAAGT CCCACACAGC-3'; reverse: 5'-TCAGCAGAGTGAGCAGAAAGAT-3'). Transcript levels in samples were investigated using a ViiA 7 Real-Time PCR System and compared to the transcript of ribosomal protein 18S as a housekeeping control. A minimum of five replicates of all samples were analyzed.

2.4 | Whole mount and histological staining

For *whole mount staining*, E15.5 and E18.5 embryos were harvested, skinned, eviscerated, and fixed in 95% ethanol overnight followed by 95% acetone overnight. Specimens were stained with Alcian Blue for cartilage (0.03% in acetic acid/95% ethanol—1:5 ratio), cleared in 1% KOH, and subsequently stained in Alizarin Red for bone (0.01% in KOH).

For *immunohistochemistry staining*, tissue was harvested, fixed in formalin, decalcified in 12% ethylenediaminetetraacetic acid (EDTA) (pH 7.4), and paraffin-embedded. Histological sections were cut 4- μ m thick and paraffin was removed in xylene, followed by rehydration with a graded ethanol series (100%, 95%, 90%, and 70%) for 3 min each. Specimens were treated with proteinase K for 15 min for antigen retrieval and incubated with 3% H₂O₂ for 15 min to quench endogenous peroxidase activity. Specimens were then blocked for 30 min using 1% BSA blocking buffer (Sigma-Aldrich). Primary antibodies against mouse *Metrn1* and isotype controls including rat immunoglobulin G (all antibodies were purchased from R&D Systems) were applied as per manufacturer's guidelines and incubated at 37°C for 2 h. This process was followed by incubation with a corresponding anti-rat secondary antibody for 30 min at 37°C. Specimens were developed using DAB Substrate Kit (Vector Laboratories) and counterstained using Mayer's hematoxylin (Sigma-Aldrich).

2.5 | Anatomical measurements

Embryonic femurs of E15.5 and E18.5 mice were stained as described above and dissected and subsequently measured under the dissection microscope. For postnatal measurements, body weight was measured on a digital scale, body length was measured from nose to tip of tail, and the lengths of isolated femur and tibiae were measured using Vernier calipers.

2.6 | μ CT analysis of skeletal development

Femurs of 6-week-old mice were dissected of soft tissue and fixed in formalin. μ CT analysis was conducted using a Scanco vivaCT 80 (Scanco Medical) at a scan resolution of 8 μ m. For trabecular analysis, bones were scanned for a 2 mm region, 2 mm proximal from the femoral condyle growth plate, and assessed for percent bone volume per total volume (%BV/TV), trabecular number (Tb. N) in mm⁻¹, and trabecular thickness (Tb. Th) in mm. For cortical analysis, bones were scanned for a 2 mm region, at the mid-point of the diaphysis, and assessed for cortical thickness (Ct. Th) in mm. Similarly, lumbar vertebrae of 16-week-old mice were dissected, fixed in formalin and scanned at 10 μ m resolution, as previously described.¹⁴ The central 1 mm region inside the L5 vertebra was examined to calculate trabecular bone parameters.

2.7 | Biomechanical testing of intact femora

The right femur from male and female mice were harvested following euthanasia, wrapped in saline-soaked gauze and frozen at -20°C until the day of testing. The specimens were gradually brought to room temperature and loaded to failure in a Bose electromechanical testing platform under 3-point bending, as previously described.^{14,15}

2.8 | Fracture surgery

Fractures were performed as previously described.^{16,17} Briefly, 4-month-old mice were anesthetized and the surgical area proximal to the knee was shaved and disinfected. Following an incision, a hole was drilled into the tibial plateau, and a 0.7-mm stainless steel pin was placed into the medullary cavity and cut flush with the tibial plateau. A tibial fracture was induced midshaft using blunt scissors, and the incision was closed using wound clips. For analgesia, 0.5 mg/kg buprenorphine-sustained release was administered subcutaneously at the beginning of the procedure. To investigate the ability of *Metrn1* to improve fracture healing, 4-month-old male mice underwent fracture surgery and either AAV8-CMV-*mMetrn1* (*Metrn1*-AAV) or AAV8-CMV-eGFP (GFP-AAV) was injected into the blood clot which forms at the site of injury. To measure the amount of *Metrn1* produced at the site of fracture, lysates of fracture calluses were assessed by *Metrn1* ELISA (R&D Systems).

2.9 | Analysis of fracture healing

Fracture calluses were dissected and fixed in 10% Zn-formalin at room temperature for 5 days. μ CT analysis was conducted using a Scanco vivaCT 80 (Scanco Medical) at a scan resolution of 8 μ m. Fractured tibiae were scanned and the midpoint of the fracture callus was identified by meticulously assessing the radiographic slices within the fracture callus—this could be determined by scanning through the slices of the callus and visually identifying the proximal and distal borders of intact cortical bone within the fracture callus. These boundaries represent the entire fracture region. The midpoint of this fracture region was defined as the fracture site. Calluses were analyzed 1 mm proximal and 1 mm distal from the fracture site and assessed for TV and BV in mm³, percentage of BV per TV, and bone mineral density in mg HA/mm³. Fixed fracture calluses were then decalcified using 12% EDTA at pH 7.4, cleared of EDTA, and embedded into paraffin. Sections were cut at a thickness of 5 μ m and stained using Alcian blue/hematoxylin/Orange G (MilliporeSigma) to visualize bone and cartilage. TRAP staining was performed as previously described.¹⁸ TRAP-positive cells were quantified as the percentage of osteoclast surface to bone surface. A minimum of 5 sections were used to conduct computer-assisted histomorphometry analysis, and results were presented as an amount relative to the total area of the fracture callus.

2.10 | RNA sequencing

Tibial diaphyseal bone samples from 12-week-old male *Metrn1*^{-/-} and *Metrn1*^{+/+} mice (n = 8/group) were rapidly collected at necropsy, as previously described.¹⁹ Briefly, bone marrow was flushed with high speed centrifugation and the remaining hollow specimens were frozen in liquid nitrogen. Total RNA was extracted with phenol-chloroform separation and on-column purification. RNA-seq libraries were generated with the Illumina TruSeq Kit according to the manufacturer's instructions. Libraries were sequenced to generate >20 million 50 bp paired-end reads. Raw reads were aligned to the mouse reference genome with RUM²⁰ and analyzed with edgeR²¹ for differential expression of genes.

2.11 | Data analysis

All statistical analysis was performed using GraphPad PRISM 5 (version 5.01) and R. Data are expressed as mean ± 95% confidence interval. For in vitro work (tissue culture), groups were compared using independent two tailed *t* tests. For in vivo work (including developmental measurements, μ CT scans, and mechanical testing), a multivariate ANOVA was conducted with a Tukey post-hoc test. Statistical significance was assigned to *p* values less than 0.05.

3 | RESULTS

3.1 | *Metrn1* is expressed in skeletal elements during development, maturation, and growth

The spatial pattern of *Metrn1* expression during development, growth, and maturation has not been reported. We bred C57BL/6 J mice and investigated *Metrn1* expression at various stages of development. Limbs from E15.5 and E18.5 mice were harvested, fixed, and underwent paraffin-embedded sectioning. *Metrn1* expression was visualized using immunohistochemistry. The perichondrium and the primary ossification center were positive for *Metrn1* staining in both E15.5 and E18.5 mice (Figure 1A,B and Figure S1).

Expression of *Metrn1* during skeletal growth was investigated in 6-week-old mice. Femurs were harvested, fixed, decalcified, and underwent paraffin-embedded sectioning. Immunohistochemical labeling showed *Metrn1* expression within the growth plate (Figure 1C and Figure S1), and in the cells of the metaphysis but not in the cells of the diaphysis (Figure S2). These findings confirm the expression of *Metrn1* during development, growth, and maturation within the skeleton.

In addition to histologic analyses, we re-evaluated single cell RNA-seq data we previously generated using cells from neonatal mouse calvaria²² to determine the relative expression of *Metrn1* in

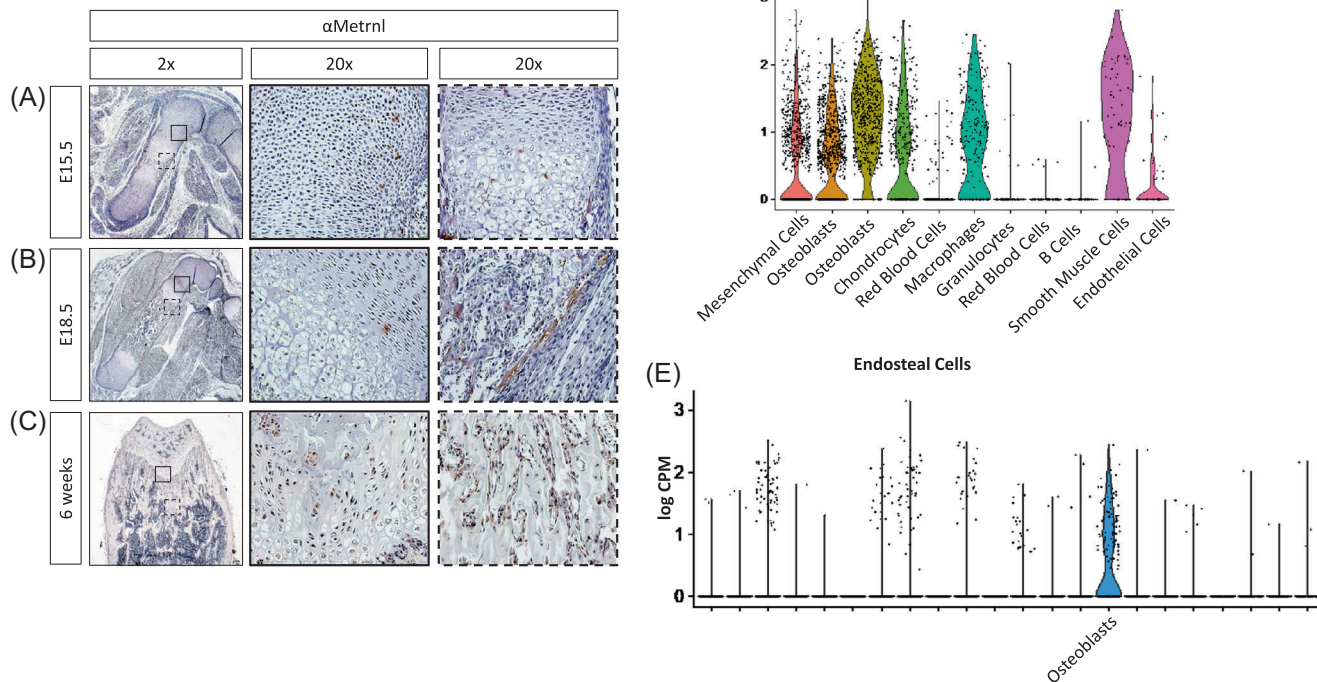


FIGURE 1 *Metrn1* is expressed in skeletal elements during development and throughout skeletal maturation and growth. Immunohistochemical staining was performed on the hind limbs of C57BL/6J mice at (A) E15.5, (B) E18.5, and (C) 6 weeks. A magnification of the growth plates is highlighted by a solid square (A,B,C), the primary ossification center by a dotted square (a), and the perichondrium by a dotted square (b). (D) Re-evaluation of previously published single cell RNA-seq data show high *Metrn1* expression in osteoblasts and other cell types from neonatal mouse calvaria [21]. (E) Single cell RNA-seq data from diaphyseal bone samples show higher expression of *Metrn1* in osteoblasts than all other cell types

distinct skeletal cell types. We detected *Metrn1* expression in mesenchymal-lineage cells (with the highest apparent expression in osteoblasts), macrophages, and smooth muscle cells (Figure 1D). Consistent with these findings, *Metrn1* expression within skeletally mature mouse diaphyseal bones was highest in mature osteoblasts (Figure 1E).

3.2 | *Metrn1* promotes in vitro osteoblast differentiation

Metrn1 expression during skeletal development and growth was primarily observed in regions adjacent to osteoblast differentiation and activity. To investigate the potential effect of *Metrn1* on osteoblast biology, bone marrow stromal cells were cultured for 7 days to allow for adherence and differentiated in osteogenic media for 14 days in the presence of vehicle or recombinant *Metrn1* (r*Metrn1*). r*Metrn1* treatment increased ALP staining (Figure 2A), indicating increased osteoblastic differentiation. Furthermore, Von Kossa (VK) staining was increased in r*Metrn1*-treated wells, indicating increased mineral formation (Figure 2A,B). These effects were further confirmed using RT-PCR analysis of osteogenic transcripts from cultures. r*Metrn1*-treatment of osteogenic cultures increased *Alp* transcript 2.5-fold, *Col1* transcript 2-fold, and *Ocn* transcript 1.5-fold (Figure 2C).

Furthermore, bone marrow stromal cells from mice in which *Metrn1* expression had been ablated displayed decreased osteogenic ability. Cultures were again adhered and then differentiated in osteogenic media. Cultures derived from *Metrn1* knockout mice displayed decreased ALP and VK staining (Figure 2D,E). Accordingly,

osteogenic transcript levels within these cultures were lower than cells from littermate controls (Figure 2F). Importantly, haploinsufficiency did not affect in vitro osteoblast differentiation (Figure S3). Collectively, these findings indicate *Metrn1* to be a pro-osteogenic factor inducing increased osteoblast differentiation and activity in vitro.

3.3 | Loss of *Metrn1* expression does not affect skeletal development or growth

We have shown that *Metrn1* is expressed during development and growth of the skeleton and that expression and/or exogenous addition of *Metrn1* is osteoinductive, leading to increased osteoblast differentiation and activity in tissue culture systems. We next performed whole mount skeletal staining with Alizarin red and Alcian blue and subsequently assessed skeletal morphology to determine whether *Metrn1* plays a role in skeletal development. Littermate *Metrn1*^{+/+}, *Metrn1*^{+/-}, and *Metrn1*^{-/-} embryos were harvested at E15.5 and E18.5, dissected, fixed, and underwent whole mount staining (Figure 3A,B). Whole mounts revealed no gross morphologic differences across genotypes and all mice appeared to be skeletally normal and healthy. Furthermore, in-depth investigation of femoral staining indicated no differences in patterning and growth (Figure 3A,B lower insets). The relative lengths of dissected femurs were determined (approximately 1.0 at E15.5 and 1.1 at E18.5 for all genotypes—Figure 3C and 3E) and the ratio of mineralized region within the bone was calculated (approximately 33% for E15.5 and 50% for E18.5 for all genotypes—Figure 3D and 3F).

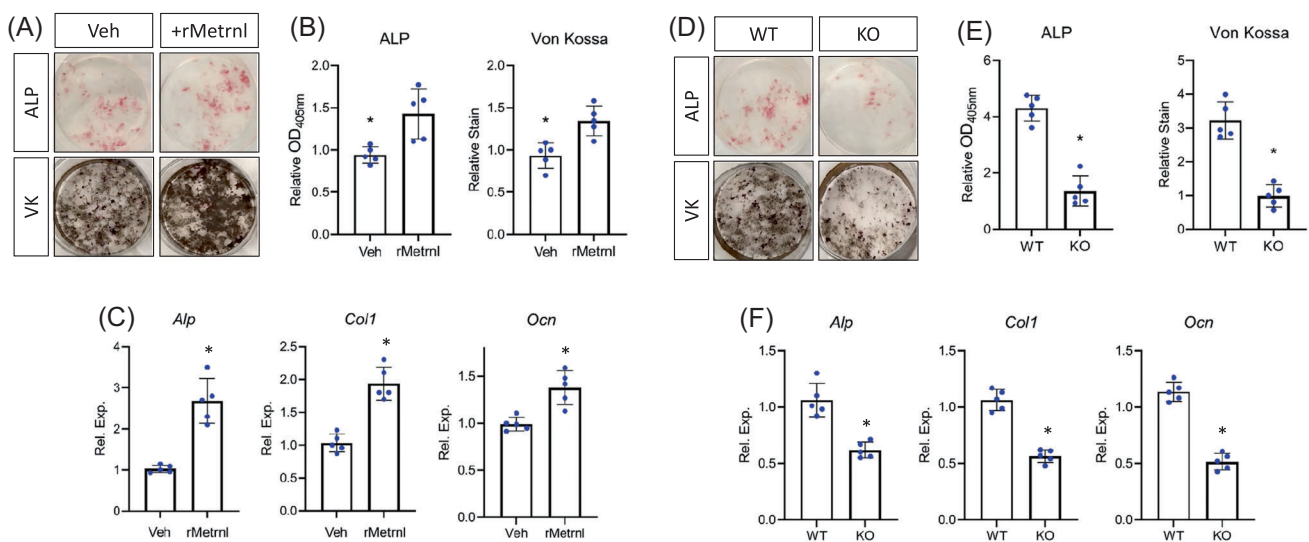


FIGURE 2 *Metrn1* promotes osteoblast differentiation and activity in vitro. Bone marrow stromal cells from 4-month-old mice were cultured and differentiated in osteogenic media. (A) Cultures from C57BL/6 mice were treated with either vehicle or r*Metrn1* throughout differentiation and stained for alkaline phosphatase (ALP) or mineral (Von Kossa—VK). (B) Quantification of stains and (C) levels of osteogenic transcripts were measured. (D) Cultures from *Metrn1*^{+/+} or *Metrn1*^{-/-} mice were differentiated and stained for alkaline phosphatase (ALP) or mineral (Von Kossa—VK). (E) Quantification of stains and (F) levels of osteogenic transcripts were measured. *n* = 5, data are expressed as mean ± 95% confidence interval, **p* < 0.05.

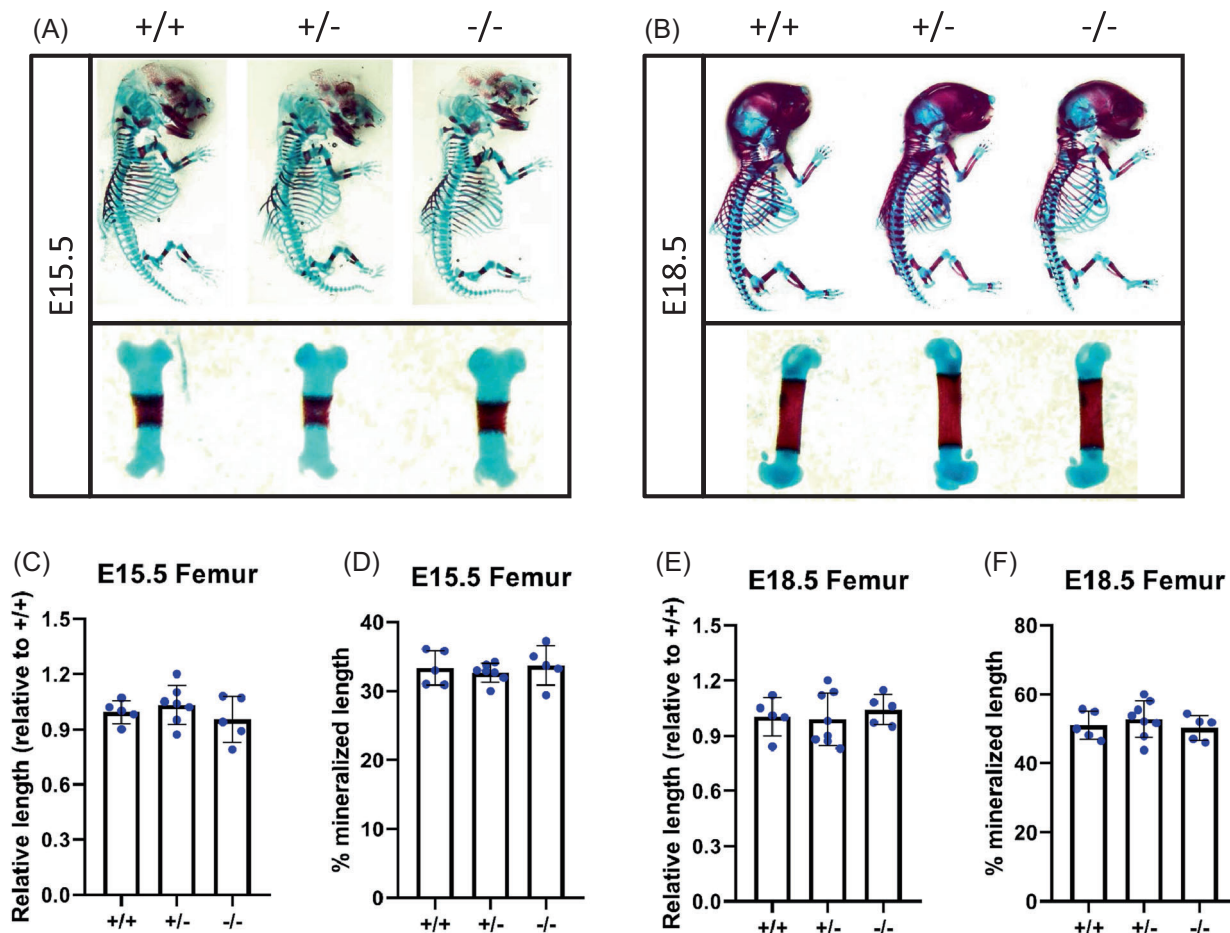


FIGURE 3 Loss of *Metrn1* expression does not affect skeletal development. *Metrn1*^{+/-} × *Metrn1*^{+/-} breeding pairs were used to generate wildtype, haplotype, and knockout progeny. Skeletons and femurs of (A) E15.5 mice and (B) E18.5 mice underwent whole mount staining (Alizarin red, bone; Alcian blue, cartilage). Relative femur length and relative mineralization length of E15.5 pups (C,D) and E18.5 pups (E,F) was measured. *n* = 5, data are expressed as mean ± 95% confidence interval

To determine the effect of *Metrn1* on postnatal development and growth, we investigated 6-week-old *Metrn1*^{+/+}, *Metrn1*^{+/-}, and *Metrn1*^{-/-} mice using gross anatomical assessment, μ CT analysis, and histological methods. The weight of the mice differed by sex; however, there were no significant differences by genotype (males weighed approximately 22.5 g for all genotypes and females weighed approximately 18.0 g for all genotypes—Figure 4A). Likewise, the length of the mice were similar (approximately 16.0 cm for males of all genotypes and approximately 15.0 cm for females of all genotypes—Figure 4B), as was the femur length (approximately 14.0 mm for males of all genotypes and approximately 13.5 mm for females of all genotypes—Figure 4C) and the tibia length (approximately 16.5 mm for males of all genotypes and approximately 15.5 mm for females of all genotypes—Figure 4D).

Using μ CT analysis, we investigated the role of *Metrn1* specifically on bone development and growth (Figure 4E). Bone metrics were calculated within the femurs of 6-week-old *Metrn1*^{+/+}, *Metrn1*^{+/-}, and *Metrn1*^{-/-} mice. For assessment of trabecular bone, transverse sections were analyzed for a 2 mm segment located 2 mm distal to the femoral condyle growth plate. The BV/TV (approximately 0.09 for all genotypes—Figure 4F), the Th. N

(approximately 1.91/mm—Figure 4G), and the Th. Tb (approximately 40 μ m for all genotypes—Figure 4H) was consistently similar for *Metrn1*^{+/+}, *Metrn1*^{+/-}, and *Metrn1*^{-/-} mice. For assessment of cortical bone, we scanned and assessed a 2 mm region at the mid-point of the diaphysis. The cortical thickness (Ct. Th) was similar for all genotypes (approximately 140 μ m—Figure 4I). Importantly, TRAP staining indicated no significant difference in osteoclast activity or osteoclast number (Figure S4). Consistent with these findings, we did not detect changes in trabecular bone mass in skeletally mature mice either: μ CT analysis of L5 vertebra from 4-month-old mice revealed differences between male and female mice, but no changes due to loss of *Metrn1* (Figure 4J–L). Collectively, these data indicate that global loss of *Metrn1* expression does not result in a negative effect on the skeleton.

3.4 | *Metrn1* expression is dispensable for intact bone strength

We have shown that *Metrn1* is expressed during bone development particularly by osteoblasts in vivo and promotes osteoblast

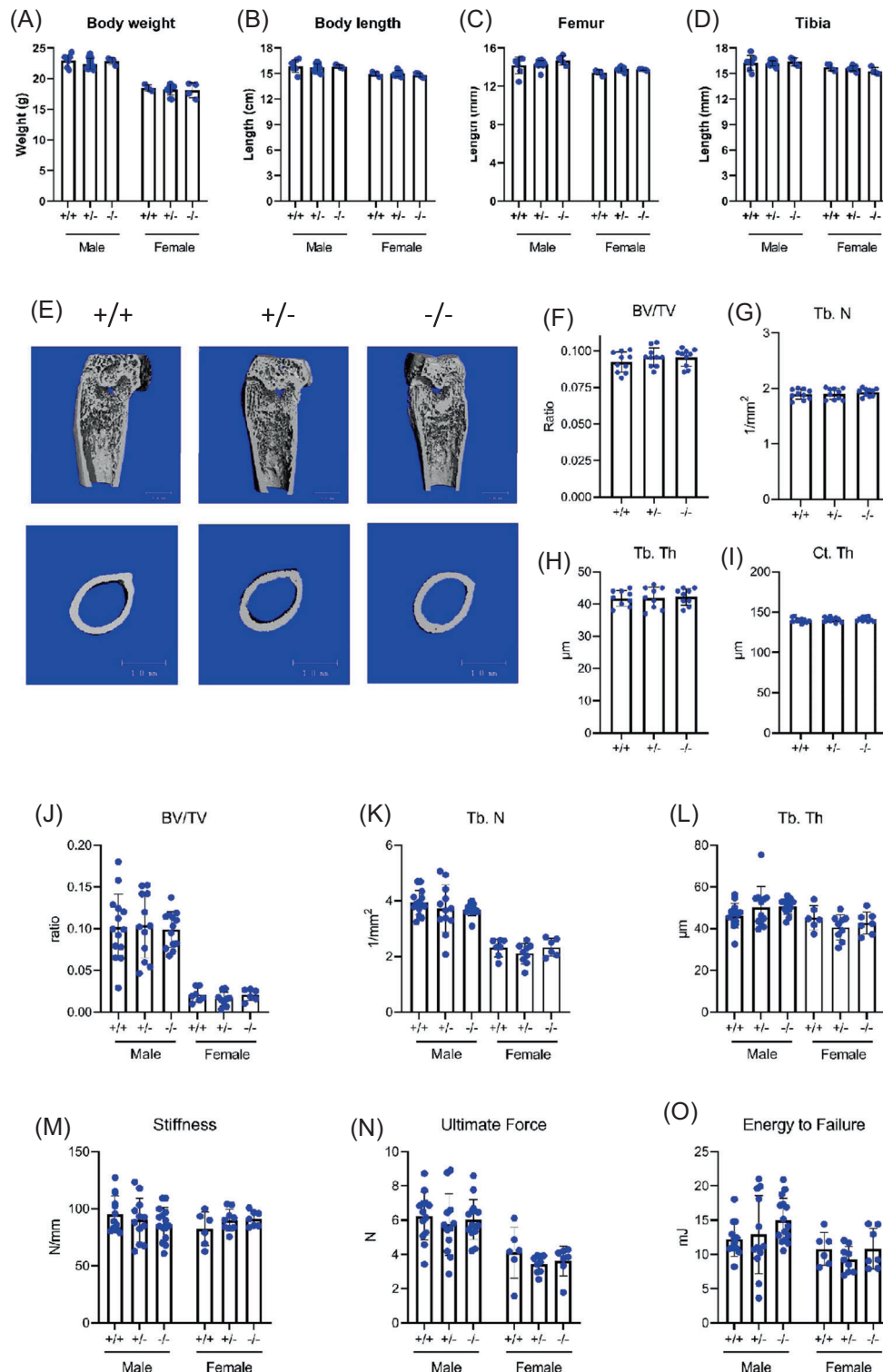


FIGURE 4 Loss of *Metrn* expression does not affect skeletal growth. 6-week-old *Metrn*^{+/+}, *Metrn*^{+/-}, and *Metrn*^{-/-} mice were investigated for (A) body weight, (B) body length, (C) femoral length, and (D) tibial length based on genotype and sex. (E) Isolated femurs underwent μ CT analysis to assess trabecular and cortical bone metrics. (F) Trabecular bone volume/total volume (BV/TV), (G) trabecular number (Tb. N), (H) trabecular thickness (Tb. Th), and (I) cortical thickness (Ct. Th) were measured ($n = 10$, data are expressed as mean \pm 95% confidence interval, $*p < 0.05$). Trabecular bone properties of L5 vertebra were assessed using micro-CT to determine (J) trabecular bone volume/total volume (BV/TV), (K) trabecular number (Tb. N), and (L) trabecular thickness (Tb. Th) ($n = 6-14$). Biomechanical properties of 4-month-old mouse femora were also evaluated under destructive 3-point-bending testing; (M) stiffness (N) ultimate force, and (O) energy to failure were measured ($n = 6-15$). μ CT, micro-computed tomography

differentiation in vitro. As osteoblasts are primarily responsible for bone formation during development and regeneration, we next investigated the potential role of *Metrn1* in modulating bone strength. We performed 3-point bending tests of femurs from 4-month-old *Metrn1*^{+/+}, *Metrn1*^{+/-}, and *Metrn1*^{-/-} mice. No differences were noted in structural stiffness with respect to sex or genotype (mean for all groups approximately 90 N/mm, $p = 0.78$) (Figure 4M). Wilcoxon rank sum test revealed sex-related differences in ultimate force (mean for males: 19.2 N, mean for females 16.2 N, $p = 0.003$) (Figure 4N) and energy to failure (mean for males: 13.5 mJ, mean for females: 10.2 mJ, $p = 0.004$) (Figure 4O) but no genotype-related differences were found for any of the biomechanical endpoints. These results indicate that loss of *Metrn1* does not compromise the biomechanical properties of long bones.

3.5 | *Metrn1* expression is dispensable for normal fracture healing

We next investigated *Metrn1* expression in the healing tibial fracture calluses of 4-month-old-C57BL/6 mice. Fracture calluses were harvested at various time points and RT-PCR was used to measure *Metrn1* transcript levels in healing tissue (Figure 5A). *Metrn1* was strongly expressed by cells within the callus and reached a maximum 14 days postfracture. Likewise, immunohistochemistry staining of these calluses revealed *Metrn1* expression (Figure 5B), further confirming that *Metrn1* is expressed in the 14-day fracture callus.

Subsequently, we examined healing after tibial fracture surgery in 4-month-old *Metrn1*^{+/+}, *Metrn1*^{+/-}, and *Metrn1*^{-/-} mice with μ CT analysis, histological techniques, and mechanical testing (Figure 5C). Limbs were harvested 21 days after injury and these fracture calluses were scanned (Figure 5D). In all groups, healing tissue displayed similar levels of tissue mineral density (TMD—approximately 315 mg HA/cm³—Figure 5E) and bone volume relative to total volume (BV/TV—approximately 0.36—Figure 5F). We stained paraffin-embedded sections from healing tibiae with Alcian Blue/Orange-G/Hematoxylin (Figure 5G). Mechanical testing of 28-day fracture calluses demonstrated no differences neither in structural stiffness (approximately 21 N/mm—Figure 5H) nor in force to refracture (approximately 78 N—Figure 5I). Furthermore, to investigate *Metrn1*'s effect on osteoclasts during fracture healing, we performed TRAP staining on 21-day fracture calluses. Both TRAP staining and quantification of osteoclast number per bone surface showed no significant difference in response to loss of *Metrn1* expression (Figure 5J).

Stemming from our findings that exogenous *Metrn1* increases osteoblast differentiation in vitro, we next tested whether increased levels of *Metrn1* promote bone regeneration. We treated 4-month-old mice with AAV-GFP or AAV-GFP-*Metrn1* at the time of fracture. In one cohort of mice, fracture calluses were harvested 14 days postinjury and the *Metrn1* levels were measured using ELISA. *Metrn1* levels were approximately two times higher in AAV-GFP-*Metrn1* treated mice (Figure 5K). Micro-CT analysis at 21 days after fracture injury indicated no change in the total volume or amount of bone

deposited in the fracture callus. Furthermore, AAV-GFP-*Metrn1* treatment did not lead to significant changes in structural stiffness or the ultimate force required to re-fracture of the fractured limb (Figure 5L). Collectively, these findings demonstrate that although *Metrn1* is expressed in the fracture callus, it does not alter bone fracture healing.

3.6 | Loss of *Metrn1* does not alter the bulk transcriptome of diaphyseal bone

Using bulk RNA sequencing, we verified deletion of the 2nd exon within the *Metrn1* gene of *Metrn1*^{-/-} mice. This resulted in an alternate transcription event with a nonsense protein product (Figure 6A). Differential expression analysis revealed that $n = 35$ diaphyseal bone transcripts were altered in *Metrn1*^{-/-} mice compared to *Metrn1*^{+/+} mice, following correction for multiple hypothesis testing ($p < 0.05$, Figure 6B). Fifteen of these were protein-coding transcripts and included *Abcg3*, *Slc15a5*, *Apo11a*, and *Ilgad* (encoding the myeloid cell marker Cd11d, Figure 6C). However, we failed to identify changes in any known markers of bone formation or resorption (such as *Bglap*, *Col1a1*, or *Acp5*), consistent with the lack of an apparent phenotype in our biomechanical and μ CT-based phenotyping experiments.

4 | DISCUSSION

Bone development and regeneration involve diverse cell types and signaling molecules. In our previous work using conditioned-media models, *Metrn1* was identified as a candidate molecule which may improve osteoblast differentiation and bone formation.¹ Indeed, here we demonstrate that *Metrn1* is expressed during development and during fracture healing at regions of osteoblast activity and subsequent bone deposition. Furthermore, our in vitro models demonstrate that *Metrn1* treatment of differentiating bone marrow stromal cells increases osteoblast differentiation and activity, while loss of *Metrn1* expression inhibits mineralization. Interestingly, our findings conflict with those of Gong et al.,² where *Metrn1* expression was found to be a negative effector of osteoblast differentiation in vitro. However, this group's exclusive use of cell lines and expression vectors to over-express *Metrn1* (as opposed to our use of primary cells) is a potential reason for discrepancies between our findings. Importantly, the *Metrn1* expression pattern reported by Gong et al.² in rat skeletal tissues is consistent with our findings in mice, wherein we show that *Metrn1* expression is highest in areas of active bone deposition and osteoblasts exhibit the highest relative expression of *Metrn1* compared to other cell types. Evaluation of our previously published single cell RNA-seq data also shows that *Metrn1* is expressed by a more diverse group of cells (that include osteoblast-lineage cells and macrophages) in neonatal mouse calvaria compared with adult diaphyseal bone; however, we did not observe any gross abnormalities in *Metrn1*-null mouse skulls. These data indicate that

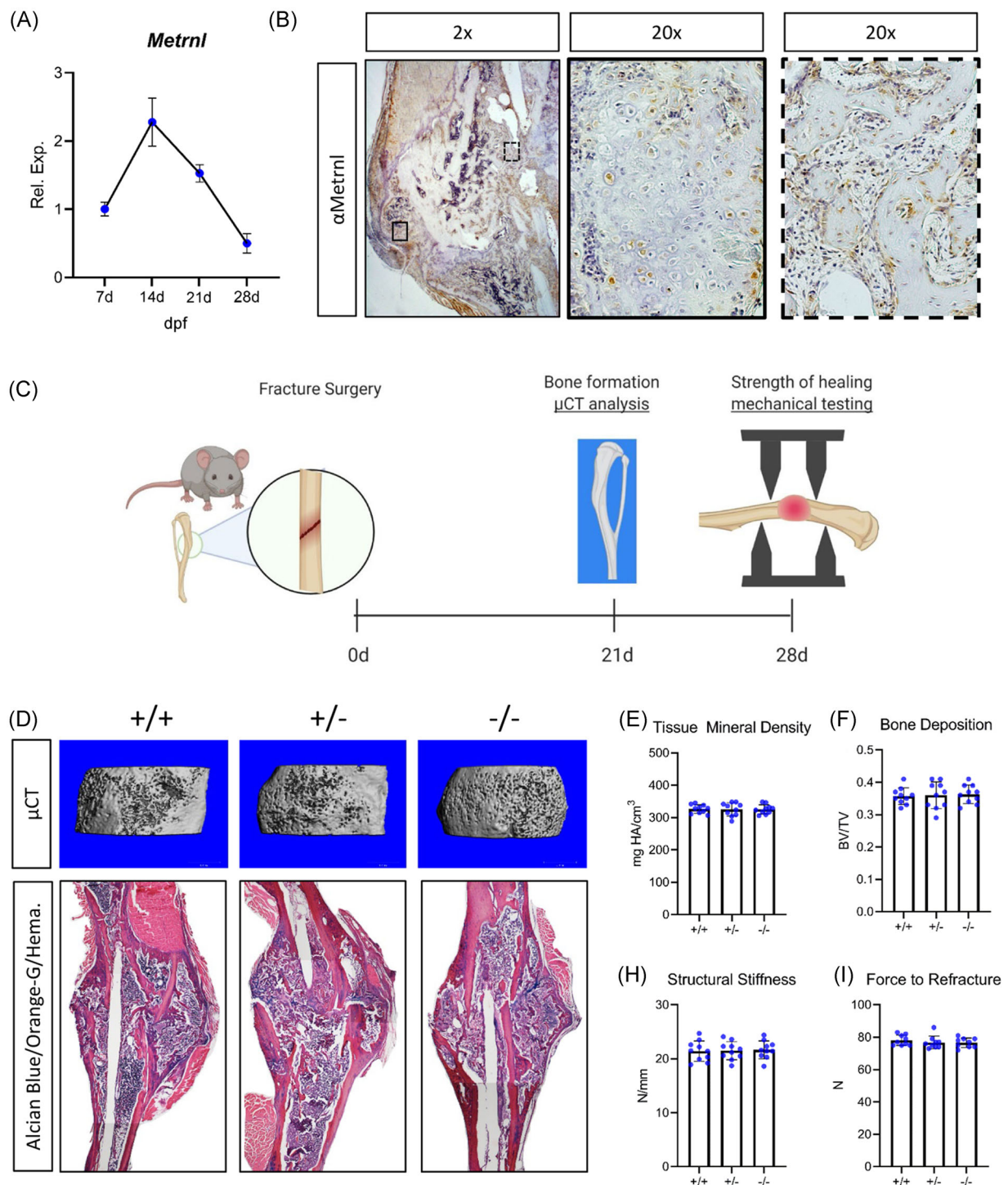


FIGURE 5 *Metn1* expression is dispensable for normal bone fracture healing. (A) *Metn1* expression was assessed within the fracture callus during repair. (B) IHC for *Metn1* in 14-day fracture calluses was performed. (C) 4-month-old *Metn1*^{+/+}, *Metn1*^{+/-}, and *Metn1*^{-/-} mice underwent tibial fracture and fractured limbs were isolated 21 and 28 days postinjury. (D) 21-day fracture calluses were investigated using micro-CT analysis to determine (E) tissue mineral density (TMD) and (F) bone volume relative to total volume (BV/TV). (G) Histological sections of healing fractures were stained with Alcian Blue/Orange G/Hematoxylin. Mechanical testing was performed on limbs harvested 28 days after injury to determine (H) structural stiffness and (I) force to refracture. For IHC and rt-pcr, $n = 5$. For μ CT and histology, $n = 10$. Data are expressed as mean \pm 95% confidence interval. μ CT, micro-computed tomography; IHC, immunohistochemistry

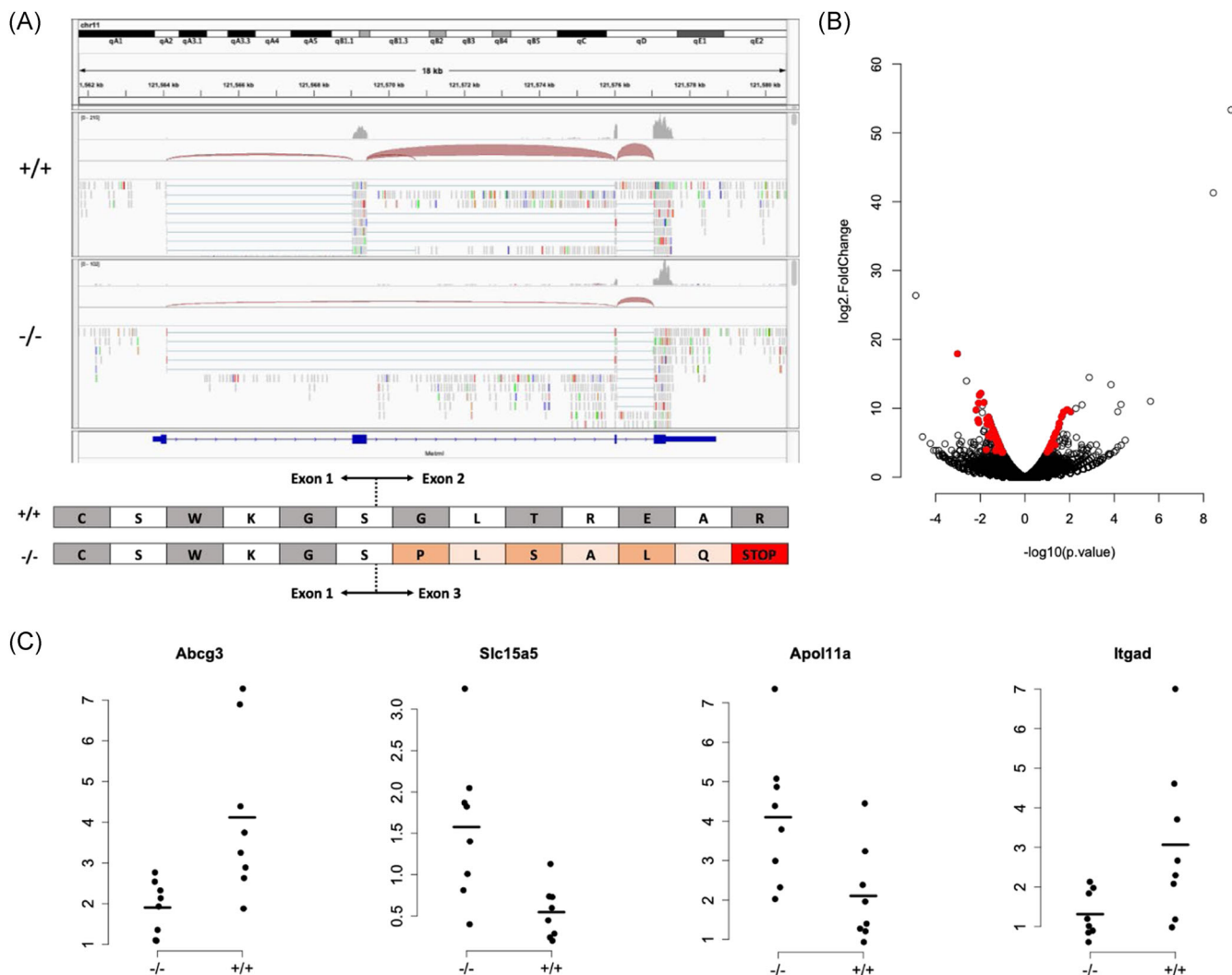


FIGURE 6 Loss of *Metrn1* does not induce transcriptional changes associated with bone formation. (A) Integrated Genomics Viewer screenshot of representative RNA-seq data from *Metrn1*^{+/+} and *Metrn1*^{-/-} bone specimens. Deletion of exon 2 results in an alternate transcription event, which introduces a premature stop codon, as shown in the diagram below. (B) Volcano plot depicting significant changes (red dots, $p < 0.05$ after correction for multiple hypothesis testing) in $n = 35$ transcripts due to loss of *Metrn1* expression. (C) Four representative transcripts with a significant change in abundance in *Metrn1*^{-/-} mouse diaphyseal bones

Metrn1 expression may vary in the skeleton with respect to developmental stage and anatomic location.

Despite this expression pattern and our finding that *Metrn1* can affect osteoblasts in vitro, loss of *Metrn1* expression in mice did not translate to a bone phenotype. We have verified this using two independent knockout mouse models and by performing in-depth skeletal phenotyping with histologic imaging, biomechanical testing, and μ CT analysis. When we examined *Metrn1*^{-/-} and littermate controls during embryonic development at E15.5 (when the primary ossification center begins to form) and E18.5 (when the bone collar forms and osteoblasts have appeared) we did not find any differences in femur length and mineralization. Likewise, radiographic measurements of 6- or 16-week-old-mutant mice displayed no difference in bone volume/total volume, trabecular number, trabecular thickness, or cortical thickness from wildtype controls. One possible explanation for this observation could be dysregulation of osteoclast activity;

however, TRAP staining in 6-week-old femurs and in healing fracture calluses 21 days after injury indicated no notable change in osteoclasts due to loss of *Metrn1* expression.

We also demonstrated expression of *Metrn1* by osteoblasts in development, homeostasis, and during fracture healing. However, we did not observe a *Metrn1*-dependent phenotype in any of these processes. Interestingly, our findings are analogous to those from our earlier work on muscle development: We have previously reported *Metrn1* to be expressed by muscle cells and as in bone, loss of *Metrn1* expression in α -actin-Cre;*Metrn1*^{f/f} animals led to no changes in muscle properties (based on muscle fiber cross-sectional area and grip strength measurements).⁸

One possible reason for a lack of skeletal phenotype in *Metrn1*-null mice (despite high *Metrn1* expression in osteoblasts) is genetic redundancy. Such functional compensation can be exemplified by considering the SIBLING (small, integrin-binding ligand N-linked

glycoprotein) family of proteins that was originally thought to be associated solely with mineralized tissues but have since been found in numerous tissues and cells types.²³⁻²⁶ Among this group, bone sialoprotein was initially identified as a key bone-hydroxyapatite nucleating agent and osteopontin as a counter-acting, mineralization-inhibiting agent.²⁷⁻³⁰ Investigation of these proteins using in vitro cell-culture models confirmed strong phenotypes aligning with these corresponding assumptions/hypotheses^{31,32}; however, loss of expression of these respective genes in vivo demonstrated mice to be normal at birth and a bone phenotype was not observed until skeletal maturity.^{33,34} Since then, studies have demonstrated a more complex mechanism for this family of proteins and strongly suggest a functional redundancy among this group.³⁵⁻³⁷

Similar mechanisms of compensation may be the reason we did not observe any significant differences in bone fracture healing of *Metrn1*^{-/-} mice. We recently demonstrated *Metrn1* to play an important role in muscle regeneration. During early stages of muscle injury macrophages at the site of healing tissue secreted high levels of *Metrn1* which played a role in resolution of inflammation.⁸ Loss of *Metrn1* expression globally and specifically in macrophages (using a lysozyme-Cre model) led to prolonged inflammation at the site of injury and impaired muscle healing. Furthermore, we and others have reported a critical role for macrophages and their secretomes in bone repair. While we did observe strong *Metrn1* expression during fracture healing at both the transcript and protein level in wildtype mice (potentially due to an increased presence of osteoblasts and macrophages within the callus), loss of *Metrn1* expression in *Metrn1*^{-/-} mice did not change the amount of bone deposition or tissue mineral density 21 days after injury, nor did it change the structural stiffness and force to refracture 28 days after injury. There are numerous factors from local niche and from circulation able to alter bone regeneration that we and others have identified.^{18,38-43} Thus there could exist a compensatory mechanism amongst one or more of these factors. Furthermore, these compensating molecule(s) would likely be lacking in our in vitro culture models as the constituents of these models are more defined. This would also explain why *Metrn1* expression was dispensable for normal bone development and healing in vivo but *Metrn1* served as an osteoinductive molecule in cell culture in vitro.

Our findings show that while *Metrn1* is not necessary for the skeleton, providing it to osteoblasts in vitro improves differentiation. *Metrn1*-deficiency has no detectable effect on fracture healing, and conversely, doubling the expression of *Metrn1* within the fracture callus also does not yield a notable change in bone healing. Supplementing *Metrn1* at supraphysiologic levels can potentially improve osteoblast numbers or function (in a similar fashion to what we observed in vitro), however, further investigation is necessary to explore whether *Metrn1* holds therapeutic value for patients with skeletal disorders. As there remains a clinical need for therapeutic enhancement of bone healing and the 1-year mortality rate of hip fractures alone is reported to be 22%-40%,⁴⁴⁻⁴⁹ the osteoinductive nature of *Metrn1* may prove useful to better design treatment strategies

which focus on implantation of cells at the site of injury. However, the exact mechanism of this osteoinductive function is still unknown. Future work to better understand the pathway through which *Metrn1* promotes osteogenic differentiation, and in vivo delivery of *Metrn1* to sites of active bone formation may provide insight into its function in the body and the development of novel orthopedic therapies.

ACKNOWLEDGEMENTS

The authors would like to thank Dr. Matthew Warman for his thoughtful comments on the design and performance of the experiments. G.S.B. was supported by a Borden Scholars award, Duke Claude D. Pepper Older Americans Independence Center Pilot Award (P30AG028716), and by the NIH/NIA (R21AG067245). A.G.R. was supported by NIH/NIAMS (R01AR053237).

AUTHOR CONTRIBUTIONS

James P White, Alexander G Robling, Ugur M Ayturk, Gurpreet S Baht: designed the study; **Rong Huang, Abhinav R Balu, Kristin H Molitoris:** conducted experiments; all authors took part in data analysis and interpretation; **Gurpreet S Baht and Ugur M Ayturk:** drafted the manuscript; all authors took part in editing the manuscript. All authors have read and approved the final submitted manuscript.

ORCID

Rong Huang  <https://orcid.org/0000-0003-3748-3627>

Ugur M. Ayturk  <https://orcid.org/0000-0001-6625-2743>

Gurpreet S. Baht  <https://orcid.org/0000-0002-6827-1785>

REFERENCES

1. Vi L, Baht GS, Soderblom EJ, et al. Macrophage cells secrete factors including LRP1 that orchestrate the rejuvenation of bone repair in mice. *Nat Commun.* 2018;9:5191.
2. Gong W, Liu Y, Wu Z, Wang S, Qiu G, Lin S. Meteorin-like shows unique expression pattern in bone and its overexpression inhibits osteoblast differentiation. *PLoS One.* 2016;11:e0164446.
3. Nishino J, Yamashita K, Hashiguchi H, Fujii H, Shimazaki T, Hamada H. Meteorin: a secreted protein that regulates glial cell differentiation and promotes axonal extension. *EMBO J.* 2004;23:1998-2008.
4. Li ZY, Song J, Zheng SL, et al. Adipocyte *metrn1* antagonizes insulin resistance through PPARgamma signaling. *Diabetes.* 2015;64:4011-4022.
5. Rao RR, Long JZ, White JP, et al. Meteorin-like Is a Hormone that Regulates Immune-Adipose Interactions to Increase Beige Fat Thermogenesis. *Cell.* 2014;157:1279-1291.
6. Lee JO, Byun WS, Kang MJ, et al. The myokine meteorin-like (*metrn1*) improves glucose tolerance in both skeletal muscle cells and mice by targeting AMPK alpha 2. *FEBS J.* 2020;287:2087-2104.
7. Ushach I, Arrevillaga-Boni G, Heller GN, et al. Meteorin-like/Meteorin-beta is a novel immunoregulatory cytokine associated with inflammation. *J Immunol.* 2018;201:3669-3676.
8. Baht GS, Bareja A, Lee DE, et al. Meteorin-like facilitates skeletal muscle repair through a Stat3/IGF-1 mechanism. *Nat Metab.* 2020;2:278-289.
9. He C, He W, Hou J, et al. Bone and muscle crosstalk in aging. *Front Cell Dev Biol.* 2020;8:585644.
10. Brotto M, Bonewald L. Bone and muscle: Interactions beyond mechanical. *Bone.* 2015;80:109-114.

11. Brotto M, Johnson ML. Endocrine crosstalk between muscle and bone. *Curr Osteoporos Rep.* 2014;12:135-141.
12. Brommage R, Liu J, Hansen GM, et al. High-throughput screening of mouse gene knockouts identifies established and novel skeletal phenotypes. *Bone Res.* 2014;2:14034.
13. Ng AH, Baht GS, Alman BA, Grynblas MD. Bone marrow stress decreases osteogenic progenitors. *Calcif Tissue Int.* 2015;97:476-486.
14. Cui Y, Niziolek PJ, MacDonald BT, et al. Lrp5 functions in bone to regulate bone mass. *Nat Med.* 2011;17:684-691.
15. Sawakami K, Robling AG, Ai M, et al. The Wnt co-receptor LRP5 is essential for skeletal mechanotransduction but not for the anabolic bone response to parathyroid hormone treatment. *J Biol Chem.* 2006;281:23698-23711.
16. Huang R, Vi L, Zong X, Baht GS. Maresin 1 resolves aged-associated macrophage inflammation to improve bone regeneration. *FASEB J.* 2020;34:13521-13532.
17. Huang R, Zong X, Nadesan P, et al. Lowering circulating apolipoprotein E levels improves aged bone fracture healing. *JCI Insight.* 2019;4:274.
18. Vi L, Baht GS, Whetstone H, et al. Macrophages promote osteoblastic differentiation in-vivo: implications in fracture repair and bone homeostasis. *J Bone Miner Res.* 2015;30:1090-1102.
19. Ayturk UM, Jacobsen CM, Christodoulou DC, et al. An RNA-seq protocol to identify mRNA expression changes in mouse diaphyseal bone: applications in mice with bone property altering Lrp5 mutations. *J Bone Miner Res.* 2013;28:2081-2093.
20. Grant GR, Farkas MH, Pizarro AD, et al. Comparative analysis of RNA-Seq alignment algorithms and the RNA-Seq unified mapper (RUM). *Bioinformatics.* 2011;27:2518-2528.
21. Robinson MD, McCarthy DJ, Smyth GK. edgeR: a Bioconductor package for differential expression analysis of digital gene expression data. *Bioinformatics.* 2010;26:139-140.
22. Ayturk UM, Scollan JP, Goz Ayturk D, et al. Single-cell RNA sequencing of calvarial and long-bone endocortical cells. *J Bone Miner Res.* 2020;35:1981-1991.
23. Fisher LW, Fedarko NS. Six genes expressed in bones and teeth encode the current members of the SIBLING family of proteins. *Connect Tissue Res.* 2003;44(Suppl 1):33-40.
24. Alford AI, Hankenson KD. Matricellular proteins: extracellular modulators of bone development, remodeling, and regeneration. *Bone.* 2006;38:749-757.
25. Ogbureke KU, Fisher LW. Expression of SIBLINGs and their partner MMPs in salivary glands. *J Dent Res.* 2004;83:664-670.
26. Ogbureke KU, Fisher LW. Renal expression of SIBLING proteins and their partner matrix metalloproteinases (MMPs). *Kidney Int.* 2005;68:155-166.
27. Sodek J, Ganss B, McKee MD. Osteopontin. *Crit Rev Oral Biol Med.* 2000;11:279-303.
28. Ganss B, Kim RH, Sodek J. Bone sialoprotein. *Crit Rev Oral Biol Med.* 1999;10:79-98.
29. Baht GS, O'Young J, Borovina A, et al. Phosphorylation of Ser136 is critical for potent bone sialoprotein-mediated nucleation of hydroxyapatite crystals. *Biochem J.* 2010;428:385-395.
30. Baht GS, Hunter GK, Goldberg HA. Bone sialoprotein-collagen interaction promotes hydroxyapatite nucleation. *Matrix Biol.* 2008;27:600-608.
31. Bouet G, Boulefour W, Juignet L, et al. The impairment of osteogenesis in bone sialoprotein (BSP) knockout calvaria cell cultures is cell density dependent. *PLoS One.* 2015;10:e0117402.
32. Kusuyama J, Bandow K, Ohnishi T, et al. Osteopontin inhibits osteoblast responsiveness through the down-regulation of focal adhesion kinase mediated by the induction of low-molecular weight protein tyrosine phosphatase. *Mol Biol Cell.* 2017;28:1326-1336.
33. Malaval L, Wade-Gueye NM, Boudiffa M, et al. Bone sialoprotein plays a functional role in bone formation and osteoclastogenesis. *J Exp Med.* 2008;205:1145-1153.
34. Yoshitake H, Rittling SR, Denhardt DT, Noda M. Osteopontin-deficient mice are resistant to ovariectomy-induced bone resorption. *Proc Natl Acad Sci USA.* 1999;96:8156-8160.
35. Boulefour W, Juignet L, Verdier L, et al. Deletion of OPN in BSP knockout mice does not correct bone hypomineralization but results in high bone turnover. *Bone.* 2019;120:411-422.
36. Ling Y, Rios HF, Myers ER, Lu Y, Feng JQ, Boskey AL. DMP1 depletion decreases bone mineralization in vivo: an FTIR imaging analysis. *J Bone Miner Res.* 2005;20:2169-2177.
37. Liu T, Wang J, Xie X, et al. DMP1 ablation in the rabbit results in mineralization defects and abnormalities in haversian canal/osteon microarchitecture. *J Bone Miner Res.* 2019;34:1115-1128.
38. Baht GS, Silkstone D, Vi L, et al. Exposure to a youthful circulator rejuvenates bone repair through modulation of beta-catenin. *Nat Commun.* 2015;6:7131.
39. Clark D, Brazina S, Yang F, et al. Age-related changes to macrophages are detrimental to fracture healing in mice. *Aging cell.* 2020;19:e13112.
40. Lu C, Miclau T, Hu D, et al. Cellular basis for age-related changes in fracture repair. *J Orthop Res.* 2005;23:1300-1307.
41. Zeng Y, Shih YV, Baht GS, Varghese S. In vivo sequestration of innate small molecules to promote bone healing. *Adv Mater.* 2020;32:e1906022.
42. Yuasa M, Mignemi NA, Nyman JS, et al. Fibrinolysis is essential for fracture repair and prevention of heterotopic ossification. *J Clin Invest.* 2015;125:3117-3131.
43. Baht GS, Nadesan P, Silkstone D, Alman BA. Pharmacologically targeting beta-catenin for NF1 associated deficiencies in fracture repair. *Bone.* 2017;98:31-36.
44. Ray NF, Chan JK, Thamer M, Melton LJ 3rd. Medical expenditures for the treatment of osteoporotic fractures in the United States in 1995: report from the National Osteoporosis Foundation. *J Bone Miner Res.* 1997;12:24-35.
45. Youm T, Koval KJ, Zuckerman JD. The economic impact of geriatric hip fractures. *Am J Orthop (Belle Mead NJ).* 1999;28:423-428.
46. Roche JJ, Wenn RT, Sahota O, Moran CG. Effect of comorbidities and postoperative complications on mortality after hip fracture in elderly people: prospective observational cohort study. *BMJ.* 2005;331:1374.
47. von Friesendorff M, Besjakov J, Akesson K. Long-term survival and fracture risk after hip fracture: a 22-year follow-up in women. *J Bone Miner Res.* 2008;23:1832-1841.
48. Berry SD, Samelson EJ, Bordes M, Broe K, Kiel DP. Survival of aged nursing home residents with hip fracture. *J Gerontol A Biol Sci Med Sci.* 2009;64:771-777.
49. Elliott J, Beringer T, Kee F, Marsh D, Willis C, Stevenson M. Predicting survival after treatment for fracture of the proximal femur and the effect of delays to surgery. *J Clin Epidemiol.* 2003;56:788-795.

SUPPORTING INFORMATION

Additional supporting information may be found in the online version of the article at the publisher's website.

How to cite this article: Huang R, Balu AR, Molitoris KH, et al. The role of Meteorin-like in skeletal development and bone fracture healing. *J Orthop Res.* 2022;40:2510-2521. doi:10.1002/jor.25286